STRUCTURAL SCIENCE
CRYSTAL ENGINEERING
MATERIALS

Volume 73 (2017)

Supporting information for article:

Formation of co-racemic uranyl chromate constructed from chiral layers of different topology

Oleg Siidra, Evgeny Nazarchuk, Sergey Bocharov, Wulf Depmeier and Anastasiya Zadoya

Acta Crystallographica Section B supporting information

Formation of co-racemic uranyl chromate constructed from chiral layers of different topology

Details of corrections to the article

Oleg Siidra[a]*, Evgeni Nazarchuk[a], Sergey Bocharov[a], Wulf Depmeier[b] and Anastasiya Zadoya[a]

[a]Department of Crystallography, Saint-Petersburg State University, University emb. 7/9, St.Petersburg, 199034, Russian Federation, and [b]Institut für Geowissenschaften der Universität Kiel, Olshausenstr. 40, Kiel, D-24098, Germany

Correspondence email: o.siidra@spbu.ru

Details are given on the corrections made to Table 2 of the article by Siidra *et al.* (2017). The values of M_r , Z and D_x for compounds (1), (2) and (3) were corrected. The revised values are given below:

Compound (1): M_r = 1016.25, Z = 2.

Compound (2): M_r = 1066.12, Z = 4.

Compound (3): M_r = 1054.34, Z = 4, D_x = 2.83.

The originally published version of the article, without corrections, forms pages 3 to 13 of this document.

Acta Cryst B
STRUCTURAL SCIENCE
CRYSTAL ENGINEERING
MATERIALS

ISSN 2052-5206

Formation of co-racemic uranyl chromate constructed from chiral layers of different topology

Oleg Siidra,[a]* Evgeny Nazarchuk,[a] Sergey Bocharov,[a] Wulf Depmeier[b] and Anastasiya Zadoya[a]

[a]Department of Crystallography, Saint-Petersburg State University, University emb. 7/9, St Petersburg 199034, Russian Federation, and [b]Institut für Geowissenschaften der Universität Kiel, Olshausenstr. 40, Kiel D-24098, Germany. *Correspondence e-mail: o.siidra@spbu.ru

Received 27 September 2016
Accepted 1 December 2016

Edited by N. B. Bolotina, Russian Academy of Sciences, Russia

Keywords: layered compounds; chirality; racemates; organically templated compounds; uranium.

CCDC references: 1520397; 1520398; 1520399; 1520400

Supporting information: this article has supporting information at journals.iucr.org/b

Four new inorganic uranyl chromates were obtained by evaporation and hydrothermal methods: $[(CH_3)_2NH_2]_2[(UO_2)_2(CrO_4)_3(H_2O)](H_2O)$ (1), $K(Rb_{0.6}K_{0.4})[(UO_2)_2(CrO_4)_3(H_2O)](H_2O)_3$ (2) $[(CH_3)_3CNH_3]_2[(UO_2)_2(CrO_4)_3H_2O]$ (3), $[(CH_3)_2NH_2]_4[(UO_2)_2(CrO_4)_3H_2O]_2(H_2O)$ (4). Their structures are based on two-dimensional chiral or achiral units with the composition $[(UO_2)_2(CrO_4)_3(H_2O)]^{2-}$ and two types of topologies (*A* or/and *B*). The structural architecture of (4) is unique amongst all known uranyl-based structures, and unusual among hybrid organic/inorganic structures in general as it contains layers of identical composition, but of different topology. The unique structural configurations and non-centrosymmetry in (1) and (4) is governed by selective formation of hydrogen bonding rather than by the formation of hydrophobic and hydrophilic zones in the organic interlayer. It is shown that chiral architectures in uranyl systems may form from achiral building units as observed in (3) and (4). This is somewhat analogous to certain organic compounds, where achiral molecules are also able to form chiral layers. Within the concept of such an interpretation the structure of (3) can then be described as a racemate consisting of two *A* and *A*′ chiral layers. In a similar approach the structure of (4) can be interpreted as being formed by four chiral layers. Layer pairs *AA*′ and *BB*′ can then be considered as racemic pairs and the whole structure is a co-racemate built by a combination of two racemates. Two-stage formation can be suggested for (4).

1. Introduction

Compared with organic crystal structures which often consist of chiral molecules, such as amino acids, sugars *etc.*, chirality is arguably a much less common phenomenon in inorganic crystals. Nevertheless, there are notable exceptions, including certain zeolites and zeolite-like structures (Yu & Xu, 2008; Tang *et al.*, 2011), the vast majority of which are, however, actually achiral. It should be noted that chiral structures, or parts thereof, do not necessarily require chiral building units from which they are formed, but suitably arranged achiral entities may also result in chirality. Even if this is the case, 'right-handed' and 'left-handed' chiral entities are usually present in equal proportions and the resulting structures can be considered as racemic mixtures. Some rare exceptions from equal proportions occur among zeolites and zeolite-like structures, which thus show overall chirality (*e.g.* Dryzun *et al.*, 2009). Cases like these may have potential practical relevance, given that enantiopure or enantioenriched zeolites would allow for selective adsorption and separation of organic enantiomers, at least in principle (Zhang & Jiang, 2011; Dubbeldam *et al.*, 2014). One possible pathway to overall chiral zeolite structures is their synthesis in the presence of a

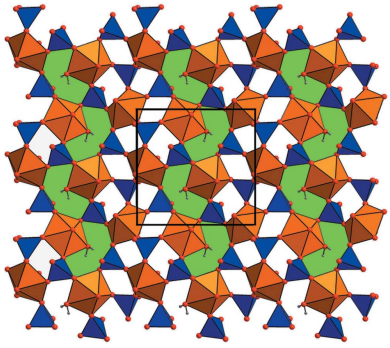

suitable structure-directing organic precursor (Lacasta *et al.*, 2011; Davis, 2014).

Another class of materials which are in some respect analogous to zeolites is that of metal–organic frameworks (MOFs), some of which are also chiral (Xu *et al.*, 2016). The versatility of MOFs relies on the fact that modification and tuning of their properties may be achieved not only by changes of their chemical composition, but also by variation of their structural architecture. Various potentially useful properties include catalytic (Ou & Wu, 2014; Leus *et al.*, 2014; Liu *et al.*, 2014), size-selective (Mallick *et al.*, 2010; Li *et al.*, 2012), non-linear optical and luminescent properties (Carrión *et al.*, 2011; Li *et al.*, 2008). Also the possibility to prepare chiral MOFs for use in the separation of enantiomers is of practical importance (Gu *et al.*, 2016). These MOFs may be formed by chiral or achiral building units (Gao *et al.*, 2004; Dong *et al.*, 2016).

In the present study we will focus on uranyl-based structures. The majority of all these structures are centrosymmetric, because of the inherently symmetric nature of the uranyl cation $(UO_2)^{2+}$. Within the last decade, however, several reports on chiral structural architectures in framework and layered uranyl-based compounds were published (Doran *et al.*, 2002; Krivovichev *et al.*, 2005, 2009; Wang *et al.*, 2010) including minerals (Burns & Finch, 1999; Plášil *et al.*, 2013). Except for uranyl-borates and -carbonates, all of them contain tridentate tetrahedral TO_4 oxoanions (T = S^{6+}, Se^{6+}, Mo^{6+}). These are arranged in layers or chains and the chirality is the result of different 'up' and 'down' orientations of TO_4 tetrahedra, defined by T^{6+}—O_t bonds (O_t = terminal oxygen, not shared between polyhedra) pointing either 'up' or 'down' with respect to the layer. Due to the strong directional anisotropy of the bond distribution in the uranyl cation, the crystal structures of these compounds are dominated by two-dimensional structural motifs. Corner- or edge-sharing between UO_n (n = 4, 5, 6) polyhedra and TO_4 tetrahedra result in hundreds of different two-dimensional structural topologies (Krivovichev *et al.*, 2007). Each one is built up by stacking layers having identical topology and composition, which often can be transformed into each other by simple symmetry operations, or by different disposition of the layers relative to each other. Note, the only example was described in the crystal structure of the mineral billietite, $Ba(UO_2)_6O_4(OH)_6{\cdot}8H_2O$, formed by two different uranyl hydroxide layers (Finch *et al.*, 2006). To the best of our knowledge, uranyl-based structures with tetrahedral oxoanions simultaneously containing two or more different layer topologies have not previously been reported. This is in contrast to oxysalts and inorganic compounds with heteropolyhedral layers where this phenomenon occurs quite frequently. Knowing the criteria which led to different layer topologies is not only interesting, but also necessary for an understanding of the different processes which are involved in the formation of uranyl compounds and affects their stability in various technical and natural systems. Such knowledge is vital for the responsible management of spent nuclear fuel and other radioactive waste in repositories. In addition to these generally accepted research directions, another worthwhile one is the synthesis and characterization of enantiopure or enantioenriched layered uranium compounds. A possible route to tackle is by employing the approach which was successfully applied in the cases of zeolites and MOFs, *viz.* using chiral or achiral organic reactants as structure-directing agents for the syntheses.

Table 1
Reagents used for the preparation of (1), (2), (3) and (4).

	(1)	(2)	(3)	(4)
$(UO_2)(NO_3)_2{\cdot}6H_2O$ (g, Vekton, 99.7%)	0.05	0.075	0.11	0.08
CrO_3 (g, Vekton, 99.5%)	0.14	0.15	0.25	0.14
tert-Butylamine (ml, Aldrich 98%)	–	–	0.025	–
Dimethylamine (ml, Aldrich 40% in H_2O)	0.05	–	–	0.10
KCl (g, Vekton, 99.5%)	–	0.05	–	–
RbCl (g, Vekton, 99.5%)	–	0.05	–	–
Distilled H_2O (ml)	10	10	10	10
Evaporation time (h)	48	96	24	48

Layers having the common composition $[(UO_2)_2(T^{6+}O_4)_3(H_2O)]^{2-}$ (T = S^{6+}, Cr^{6+}, Se^{6+}) were previously described for a number of hydrous uranyl sulfates (Thomas *et al.*, 2003; Doran *et al.*, 2003, 2004; Bharara & Gorden, 2010), uranyl chromates (Siidra *et al.*, 2012*a*) and uranyl selenates (Ling *et al.*, 2009; Krivovichev *et al.*, 2009), all of which in addition contain organic cations. Their layers were classified by Krivovichev *et al.* (2007) into three different topologies with unique black-and-white graphs. The preferred formation of one or the other topology of layers $[(UO_2)_2(SeO_4)_3(H_2O)]^{2-}$ was explained by the formation of hydrophobic and hydrophilic areas in the organic interlayer (Krivovichev *et al.*, 2009).

Here we report the syntheses and crystal structures of three new alkyl-ammonium uranyl chromates, *i.e.* $[(CH_3)_2NH_2]_2[(UO_2)_2(CrO_4)_3(H_2O)](H_2O)$ (1), $[(CH_3)_3CNH_3]_2[(UO_2)_2(CrO_4)_3H_2O]$ (3), $[(CH_3)_2NH_2]_4[(UO_2)_2(CrO_4)_3H_2O]_2(H_2O)$ (4) and a K–Rb uranyl chromate, $K(Rb_{0.6}K_{0.4})[(UO_2)_2(CrO_4)_3(H_2O)](H_2O)_3$ (2). Their structures are based on two-dimensional chiral or achiral units with the composition $[(UO_2)_2(CrO_4)_3(H_2O)]^{2-}$. Possible mechanisms of their formation and relationships with other hybrid organic/inorganic compounds are discussed. The structural architecture of (4) is unique amongst all known uranyl-based structures, and unusual among hybrid organic/inorganic structures in general, as it contains layers of identical composition, but of different topology.

2. Experimental

2.1. Synthesis

Single crystals of (1), (2), (3) and (4) were obtained by evaporation from aqueous solutions containing mixtures of reagents given in Table 1. The reaction of anhydrous CrO_3 with water results in the formation of the strong chromic acid, which in the cases of (1), (3) and (4) protonates the amines yielding the corresponding alkyl-substituted ammonium cations. A similar procedure using CrO_3 as a starting reagent

Table 2
Crystallographic data and refinement parameters for (1), (2), (3) and (4).

Experiments were carried out at 150 K with Mo $K\alpha$ radiation.

	(1)	(2)	(3)	(4)
Crystal data				
Chemical formula	$[(CH_3)_2NH_2]_2[(UO_2)_2(CrO_4)_3(H_2O)](H_2O)$	$K(Rb_{0.6}K_{0.4})[(UO_2)_2(CrO_4)_3(H_2O)](H_2O)_3$	$[(CH_3)_3CNH_3]_2[(UO_2)_2(CrO_4)_3H_2O]$	$[(CH_3)_2NH_2]_4[(UO_2)_2(CrO_4)_3H_2O]_2(H_2O)$
M_r	2032.56	355.00	274.18	2014.54
Crystal system, space group	Monoclinic, $P2_1$	Monoclinic, $P2_1/c$	Monoclinic, $P2_1/c$	Orthorhombic, $P2_12_12_1$
a, b, c (Å)	8.8638 (10), 11.1097 (13), 11.5441 (13)	11.0898 (7), 10.5667 (7), 16.2713 (10)	11.4334 (17), 11.5250 (13), 18.790 (3)	11.1281 (10), 11.152 (1), 32.850 (3)
β (°)	107.878 (2)	90.109 (1)	92.427 (5)	90
V (Å^3)	1081.9 (2)	1906.7 (2)	2473.7 (6)	4076.7 (6)
Z	1	12	15	4
D_x (g cm^{-3})	3.120	3.710	2.761	3.282
μ (mm^{-1})	16.46	20.44	14.40	17.47
Crystal size (mm)	0.28 × 0.25 × 0.20	0.34 × 0.30 × 0.27	0.26 × 0.22 × 0.19	0.25 × 0.20 × 0.17
Data collection				
Absorption correction	Multi-scan (*SADABS*; Bruker, 2012)	Multi-scan (*SADABS*; Bruker, 2012)	Multi-scan (*SADABS*; Bruker, 2012)	Multi-scan (*SADABS*; Bruker, 2012)
T_{max}, T_{min}	0.622, 0.784	0.659, 0.822	0.568, 0.841	0.640, 0.746
No. of measured, independent and observed [$I > 2\sigma(I)$] reflections	51 165, 5160, 5129	21 653, 4605, 3824	25 245, 5969, 4991	16 152, 8521, 7726
R_{int}	0.045	0.112	0.046	0.054
θ values (°)	θ_{max} = 28.0, θ_{min} = 1.9	θ_{max} = 28.0, θ_{min} = 1.8	θ_{max} = 28.0, θ_{min} = 1.8	θ_{max} = 28.0, θ_{min} = 1.2
$(\sin\theta/\lambda)_{max}$ (Å^{-1})	0.660	0.661	0.660	0.661
Refinement				
$R[F^2 > 2\sigma(F^2)]$, $wR(F^2)$, S	0.026, 0.070, 1.11	0.046, 0.115, 1.00	0.033, 0.079, 1.02	0.049, 0.111, 1.07
No. of reflections	5160	4605	5969	8521
No. of parameters	264	247	290	281
No. of restraints	1	0	0	0
H-atom treatment	H-atom parameters not refined	H-atom parameters not refined	–	H-atom parameters not refined
$\Delta\rho_{max}$, $\Delta\rho_{min}$ (e Å^{-3})	4.21, −1.81	3.20, −6.60	4.48, −3.68	2.99, −2.27
	CCDC# 1520397	ICSD# 1520398	CCDC# 1520399	CCDC# 1520400

was recently successfully employed for the preparation of a number of uranyl chromates with organic cations and new structural architectures (Siidra *et al.*, 2012*a*,*b*, 2014; Siidra, Nazarchuk, Petrunin *et al.*, 2012; Siidra, Nazarchuk, Suknotova *et al.*, 2013), and also of purely inorganic uranyl chromates (Siidra *et al.*, 2012*c*; Siidra, Nazarchuk, Kayukov *et al.*, 2013; Nazarchuk *et al.*, 2015). The solutions were left in a fume hood to evaporate over different time periods (Table 1). Note, for the synthesis of (4) the initial mixture was first placed in a 23 ml Teflon-lined steel autoclave and heated to 393 K for 48 h and then cooled to 298 K with a cooling rate of 25 K h^{-1}. Only thereafter was the resulting yellow–red solution subjected to evaporation. The products of (1), (2), (3) and (4) consisted of macroscopically similar-looking ruby-red platy crystals. These were filtered off and washed with hexane. Crystals selected for X-ray diffraction experiments were immediately sealed in an epoxy drop and mounted on glass fibers. Qualitative electron microprobe analysis (Hitachi TM-3000) revealed no other elements, except U and Cr, with atomic number greater than 11 (Na).

2.2. X-ray experiment

Data collection for crystals of (1), (2), (3) and (4) were performed on a Bruker Smart APEX II Duo X-ray diffractometer with Mo $K\alpha$ radiation at 50 kV and 40 mA. For each crystal more than a hemisphere of X-ray diffraction data was collected at 150 K with frame widths of 0.3° in ω, and with 15 s [for (1)], 15 s [for (2)], 25 s [for (3)] and 30 s [for (4)] counting time for each frame. The data were integrated and corrected for absorption using an empirical ellipsoidal model using the *APEX* and *XPREP* Bruker programs. Compounds (1), (2), (3) are monoclinic, the observed systematic absences were consistent with the space group $P2_1$ (1) or $P2_1/c$ (2) and (3) (Table 2). Compound (4) is orthorhombic, space group $P2_12_12_1$. For (1) and (4) the $|E^2 - 1|$ parameters were found to be 0.692 and 0.715, respectively, indicating a high probability for a non-centrosymmetric space group (Marsh, 1995), which was confirmed by the subsequent structure solution and refinement. The crystal of (4) was racemically twinned with a Flack parameter (Flack, 1983) x of 0.395 (1), whereas the crystal of (1) represented an almost pure absolute configuration [x = 0.092 (1)]. The *SHELX* program package was used for all structure calculations (Sheldrick, 2015). The final model included anisotropic displacement parameters for all atoms in (1), (2) and (3), but only for U and Cr in (4). Selected interatomic distances are given in Tables 3 and 4. Localization of hydrogen sites is always challenging in uranium-based compounds. It is often impossible to reliably localize and refine H atoms from the X-ray data, despite the good quality

research papers

Table 3
Selected interatomic distances (Å) for (1)–(3) (O_t = terminal oxygen atom in CrO_4; O_b = bridging oxygen atom between UrO_5 and CrO_4 polyhedra).

	(1)	(2)	(3)
U1—O11	1.804 (7)	1.774 (7)	1.775 (5)
U1—O5	1.778 (7)	1.779 (7)	1.778 (5)
U1—O7	2.361 (8)	2.344 (7)	2.348 (5)
U1—O9	2.403 (6)	2.368 (7)	2.354 (5)
U1—O6	2.362 (7)	2.355 (6)	2.357 (5)
U1—O13	2.403 (7)	2.385 (7)	2.368 (5)
U1—O15	2.390 (7)	2.412 (7)	2.403 (5)
U2—O4	1.781 (7)	1.768 (7)	1.747 (6)
U2—O3	1.799 (7)	1.766 (7)	1.796 (6)
U2—O1	2.383 (7)	2.351 (7)	2.312 (6)
U2—O10	2.388 (7)	2.419 (6)	2.345 (6)
U2—O8	2.325 (7)	2.331 (6)	2.350 (5)
U2—O2	2.337 (7)	2.332 (7)	2.377 (5)
U2—O*W*17	2.536 (7)	2.517 (7)	2.543 (6)
Cr1—O_t14	1.619 (8)	1.586 (8)	1.608 (5)
Cr1—O_{br}6	1.699 (7)	1.664 (6)	1.649 (5)
Cr1—O_{br}7	1.661 (8)	1.653 (7)	1.654 (5)
Cr1—O_{br}2	1.682 (7)	1.670 (7)	1.686 (5)
Cr2—O_t12	1.623 (7)	1.601 (8)	1.577 (7)
Cr2—O_{br}1	1.700 (7)	1.672 (7)	1.629 (6)
Cr2—O_{br}10	1.662 (7)	1.634 (7)	1.659 (6)
Cr2—O_{br}9	1.682 (7)	1.697 (7)	1.675 (5)
Cr3—O_t16	1.628 (7)	1.575 (8)	1.612 (6)
Cr3—O_{br}15	1.665 (8)	1.616 (7)	1.653 (5)
Cr3—O_{br}13	1.665 (8)	1.662 (7)	1.663 (5)
Cr3—O_{br}8	1.717 (7)	1.694 (7)	1.665 (5)

Table 4
Selected interatomic distances (Å) for (4) (O_t = terminal oxygen atom in CrO_4; O_b = bridging oxygen atom between UrO_5 and CrO_4 polyhedra).

U1—O11	1.78 (2)	U3—O21	1.76 (2)
U1—O5	1.79 (2)	U3—O26	1.77 (2)
U1—O7	2.36 (1)	U3—O27	2.36 (1)
U1—O9	2.39 (1)	U3—O18	2.36 (1)
U1—O6	2.34 (1)	U3—O20	2.38 (1)
U1—O13	2.35 (1)	U3—O24	2.40 (1)
U1—O15	2.38 (1)	U3—O31	2.42 (2)
U2—O4	1.74 (1)	U4—O22	1.76 (2)
U2—O3	1.75 (2)	U4—O23	1.77 (2)
U2—O1	2.35 (1)	U4—O19	2.33 (2)
U2—O10	2.37 (1)	U4—O29	2.35 (1)
U2—O8	2.36 (1)	U4—O28	2.35 (1)
U2—O2	2.33 (2)	U4—O30	2.38 (2)
U2—O*W*17	2.52 (2)	U4—O*W*34	2.48 (1)
Cr1—O_t14	1.59 (2)	Cr4—O_t33	1.60 (2)
Cr1—O_{br}6	1.67 (1)	Cr4—O_{br}30	1.62 (2)
Cr1—O_{br}7	1.63 (2)	Cr4—O_{br}28	1.67 (1)
Cr1—O_{br}2	1.71 (1)	Cr4—O_{br}27	1.68 (1)
Cr2—O_t12	1.61 (2)	Cr5—O_t25	1.59 (2)
Cr2—O_{br}1	1.66 (1)	Cr5—O_{br}20	1.65 (1)
Cr2—O_{br}10	1.65 (2)	Cr5—O_{br}24	1.65 (2)
Cr2—O_{br}9	1.67 (1)	Cr5—O_{br}29	1.69 (1)
Cr3—O_t16	1.59 (2)	Cr6—O_t32	1.62 (2)
Cr3—O_{br}15	1.65 (1)	Cr6—O_{br}31	1.63 (2)
Cr3—O_{br}13	1.67 (1)	Cr6–O_{br}19	1.66 (2)
Cr3—O_{br}8	1.68 (1)	Cr6—O_{br}18	1.67 (1)

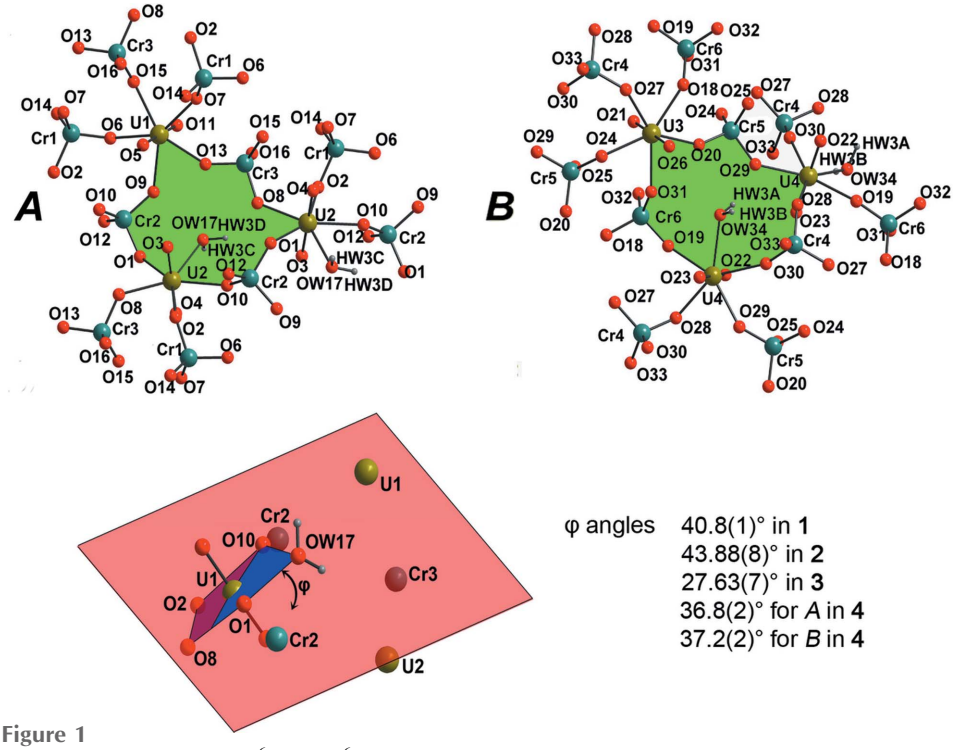

Figure 1
General projection of the U^{6+} and Cr^{6+} coordination environments forming *A* [in (1), (2), (3), (4)] and *B* [in (4) only] layers in the structures of layered uranyl chromates (above). Six-membered rings are highlighted in green. Deformation of $[(UO_2)_2(CrO_4)_3H_2O]^{2-}$ layers in (1), (2), (3) and (4) can be estimated by the φ angle between the equatorial plane of the U1-centered UrO_5 bipyramid and the plane through cations (U1, Cr2, U1, Cr3, U2 and Cr2) of six-membered rings (below). See the text for details.

and convincing results of the structure refinement. Reliable determination of hydrogen sites either of water or organic molecules in U-based compounds can be achieved *via* utilization of neutron diffraction mostly (*e.g.* Dembowski *et al.*, 2016). In (1)–(4) H sites could not be localized directly from difference Fourier maps. In the structures of (1), (2) and (4) the H atoms in water molecules and alkylammonium groups were placed geometrically and refined using a riding model. For (3), hydrogen-atom positions could not be localized.

3. Results

3.1. Basic structural features

Each of the structures of (1), (2) and (3) contain two unique U^{6+} sites, whereas there are four sites in (4) (Fig. 1, Tables 3 and 4). The U—O bond lengths within the $(UO_2)^{2+}$

uranyl groups are in the range 1.747 (6)–1.804 (7) Å. U1 [in (1), (2), (3) and (4)] and U3 [in (4)] are further coordinated by five O_{eq} atoms in the equatorial plane, thus forming UrO_5 (*Ur* = uranyl) pentagonal bipyramids. The equatorial planes of uranyl groups U2 [in (1), (2), (3) and (4)] and of U4 [in (4)] are defined by four O_{eq} atoms and one H_2O molecule [O*W*17 in (1), (2), (3) and (4), O*W*34 in (4)] and form $UrO_4(H_2O)$ pentagonal bipyramids. The U2—O*W*17 and U4—O*W*34 bonds are significantly longer [2.484 (7)–2.52 (1) Å] than other U—O_{eq} bonds [2.312 (6)–2.419 (6) Å]. UrO_5 and $UrO_4(H_2O)$ are corner-connected with five or four CrO_4 tetrahedra *via* common O atoms. Three Cr^{6+} cations in (1), (2) and (3), but six in (4) are symmetrically independent. Each CrO_4 tetrahedron is tridentate, *i.e.* it shares three corners with adjacent uranyl polyhedra. The Cr—O_{br} (O_{br} = O atom bridging between UrO_5 and CrO_4 polyhedra) bonds are longer [1.62 (2)–1.717 (7) Å] than the Cr—O_t bonds [1.586 (8)–1.62 (2) Å; O_t = terminal O atom in a chromate group]. Altogether, the UrO_5 and $UrO_4(H_2O)$ pentagonal bipyramids and the CrO_4 tetrahedra form more or less corrugated layers of composition $[(UO_2)_2(CrO_4)_3(H_2O)]^{2-}$. Six-membered rings are formed within the layer consisting of one UrO_5, two $UrO_4(H_2O)$ and three CrO_4 polyhedra, with alternating U- and Cr-centered polyhedra (Fig. 1). The water molecule of one of the $UrO_4(H_2O)$ [O*W*17 in (1), (2), (3) and (4), O*W*34 in (4)] points into the six-membered rings, and from consideration of O···O distances and angles it is likely that it acts as a donor of moderately strong hydrogen bonds with acceptors being O8 and O9 atoms bridging between the other two U-centered polyhedra and chromate tetrahedra. The Cr—O_t bonds point in two opposite directions which are essentially vertical to the layer, thus defining '*u*' and '*d*' orientations of the respective CrO_4 tetrahedra and characterizing the corresponding layers of the different compounds.

The interlayer spaces of the different compounds differ in their occupation by the various counterions [and water in (1), (2), (4)] but their distribution is rather featureless.

3.2. Individual structure descriptions

3.2.1. $[(CH_3)_2NH_2]_2[(UO_2)_2(CrO_4)_3(H_2O)](H_2O)$ (1). The structure contains one layer with chemical composition $[(UO_2)_2(CrO_4)_3(H_2O)]^{2-}$ per unit cell (Fig. 2*a*). UrO_5 pentagonal bipyramids share all five O_{eq} atoms with CrO_4 tetrahedra (2 Cr1, 1 Cr2, 2 Cr3), the $UrO_4(H_2O)$ share the four O_{eq} atoms with CrO_4 (1 Cr1, 2 Cr2, 1 Cr3), but the H_2O is dangling. Cr1O_4 and Cr3O_4 tetrahedra share corners with two UrO_5 and one $UrO_4(H_2O)$, whereas Cr2O_4 tetrahedra share corners with one UrO_5 and two $UrO_4(H_2O)$. O*W*17 has distances of 2.88 (1) and 2.83 (1) Å from O8 (bridging between U2 and Cr3) and O9 (bridging between U1 and Cr2), respectively. These distances are consistent with the assumption of moderately strong hydrogen bonds. This is corroborated by the angle O8—O*W*17—O9 of 107.7°, which might indicate rather straight O—H···O hydrogen bonds. The Cr—O_t bonds are roughly perpendicular to the $[(UO_2)_2(CrO_4)_3(H_2O)]^{2-}$ layers (Fig. 2*b*). To reveal relationships and compare with previously known $[(UO_2)_2(T^{6+}O_4)_3(H_2O)]^{2-}$ (T = S^{6+}, Cr^{6+}, Se^{6+}) layers the topology of the uranyl chromate layer in the structure of (1) can be represented by the graph representation depicted in Fig. 2(*d*). U and Cr polyhedra are symbolized by black and white nodes, respectively. Two nodes are linked by an edge if the respective polyhedra share a common corner. CrO_4 tetrahedra differ from each other by 'up' and 'down' orientations of the Cr—O_t bonds relative to the plane of the $[(UO_2)_2(CrO_4)_3(H_2O)]^{2-}$ layer. Topological analysis shows that the general

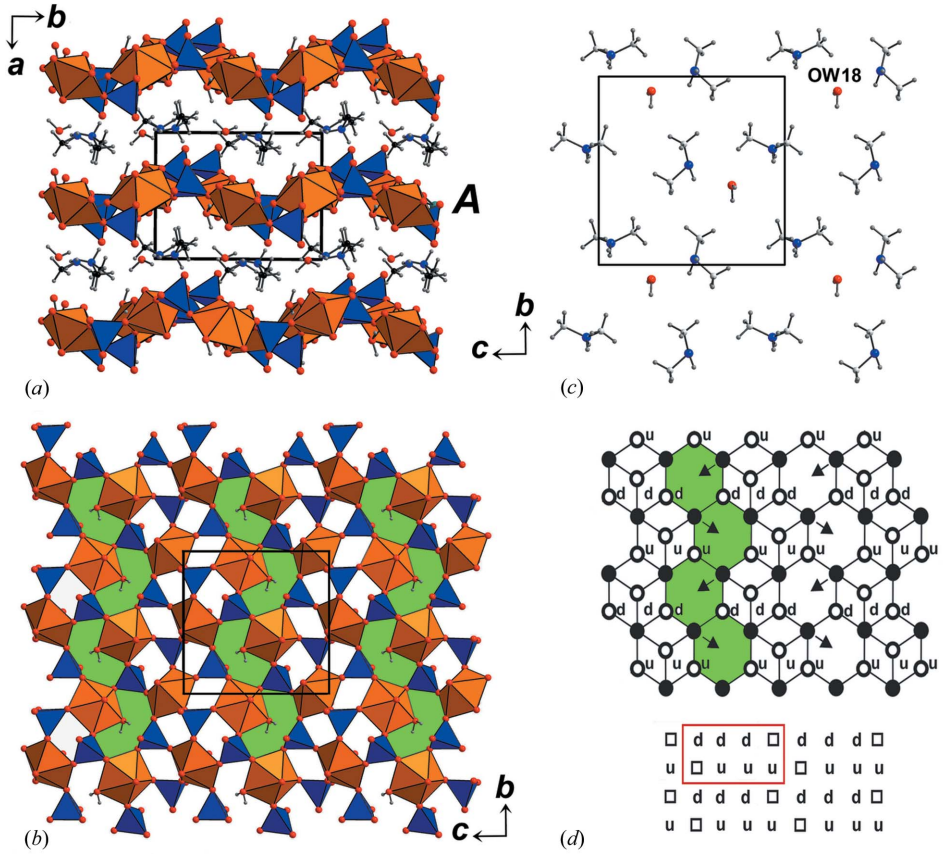

Figure 2
General projection of the structure of (1) (*a*). It contains one $[(UO_2)_2(CrO_4)_3H_2O]^{2-}$ *A* layer (*b*) per unit cell arrangement of dimethylammonium cations and O*W*18 water molecules in the interlayer (*c*). Graph of layer *A* with *u* and *d* symbols written near the white vertices (Cr atoms) (*d*). Six-membered rings form edge-sharing chains (highlighted in green). Orientations of H_2O vectors within six-membered rings are symbolized by arrows. Below the graphs the achiral orientation matrix is given.

topology of the layer in (1) is identical to previously reported ones (Thomas *et al.*, 2003; Doran *et al.*, 2003, 2004; Krivovichev *et al.*, 2009; Siidra *et al.*, 2012*a*). This type of topology (Fig. 2*d*) with six-membered rings sharing edges to form chains separated by complex chains of four-membered rings will be denoted as *A*. The orientation matrix describing the 'up' and 'down' orientations of the Cr—O_t bonds relative to the plane of the $[(UO_2)_2(CrO_4)_3(H_2O)]^{2-}$ layer is achiral (Fig. 2*d*). Note, compound (1) crystallizes in the non-centrosymmetric space group $P2_1$, whereas all other previously reported compounds with *A* layer topology crystallize in $P2_1/c$. It is also noteworthy that the unit-cell parameters of (1) are rather similar to those reported by Krivovichev *et al.* (2009) for uranyl selenates which contain exclusively layers with *B* topology to be discussed below.

The arrangement of the interlayer species dimethylammonium (DMA) and water *OW*18 is shown in Fig. 2(*c*). Some short distances between *OW*18 and O atoms of the layer point at the possibility of the formation of moderate *OW*18—H···O hydrogen bonds. Short distances between the N of the DMA are probably the result of electrostatic interactions.

3.2.2. $K(Rb_{0.6}K_{0.4})[(UO_2)_2(CrO_4)_3(H_2O)](H_2O)_3$ (2). The structure of (2) also contains layers of type *A* with the same topology and composition as that of (1) (Fig. 3*b*). However, in (2) two *A* layers are stacked onto each other whereby both are related by a 180° rotation around the 2_1 screw axis. Both layers are symmetrically equivalent under $P2_1/c$ and are denoted here *A* and *A*′ (Figs. 3*a* and *d*). The orientation matrices of the layers are achiral (Fig. 3*d*). A short distance of 2.76 (1) Å between *OW*17 and O8 is probably an indication of a moderate hydrogen bond, the corresponding distance of 3.90 (1) Å for *OW*17—O9 and the angle O8—*OW*17—O9 of about 96° would perhaps agree with the assumption of a very weak hydrogen bond. Alkali metals and water molecules (*OW*18, *OW*19, *OW*20) are located in the interlayer (Fig. 3*c*) and discussed below. There are two alkali metal sites in the structure of (2). The Rb1 site has mixed occupancy ($Rb_{0.6}K_{0.4}$) by Rb^+ and K^+ cations, whereas the K2 site is fully occupied by K^+ cations.

Note that mixed Rb1 sites are located under and above four-membered rings, whereas K1 are segregated between the six-membered rings. A similar differentiation of alkali metal sites was described previously in uranyl molybdates (Nazarchuk *et al.*, 2009). Such location of alkali metal cations is probably due to the difference in their ionic radii. Smaller K atoms are located under curved sections of the $[(UO_2)_2(CrO_4)_3(H_2O)]^{2-}$ layers, the curvature of which depends on the size and type of the incorporated cation or molecule, whereas the larger Rb^+ are associated with rigid parts formed by four-membered rings. (2) is the first 'pure' inorganic representative of the family of uranyl-based compounds with $[(UO_2)_2(T^{6+}O_4)_3(H_2O)]^{2-}$ (T = S^{6+}, Cr^{6+}, Se^{6+}) layers. All previously reported compounds of this type contained organic cations. To evaluate the influence of interlayer cations on the structure of the $[(UO_2)_2(CrO_4)_3(H_2O)]^{2-}$ layer in (2), and also in (1), (3) and (4), interpolyhedral U—O_{br}—Cr bond angles were calculated (Tables 5 and 6). It is of interest that in the structure of (2) all these angles are similar with the only exception of Cr3—O_{br}15—U1 with a value of 165.0 (5)°. In the other structures much larger differences for these values are observed. Supposedly, an explanation for this observation could be found from the fact that (2) is the only 'pure' inorganic compound in this series, whereas (1), (3) and (4) contain organic molecules. To evaluate the deformation of $[(UO_2)_2(CrO_4)_3H_2O]^{2-}$ layers in (1), (2), (3) and (4), the φ angle between the equatorial plane of the U1-centered UrO_5 bipyramid and the plane through atoms (U1, Cr2, U1, Cr3, U2 and Cr2) of six-membered rings (Fig. 1) has been calculated. The largest value of 43.88 (8)° was observed for the structure of (2) and correlates with the high degree of corrugation of $[(UO_2)_2(CrO_4)_3(H_2O)]^{2-}$ due to the presence of large K^+ and Rb^+ cations in the interlayer. The smallest value of 27.63 (7)° and thus flat layers in (3) correlates with the absence of additional water molecules in the interlayer and the presence of exclusively organic cations.

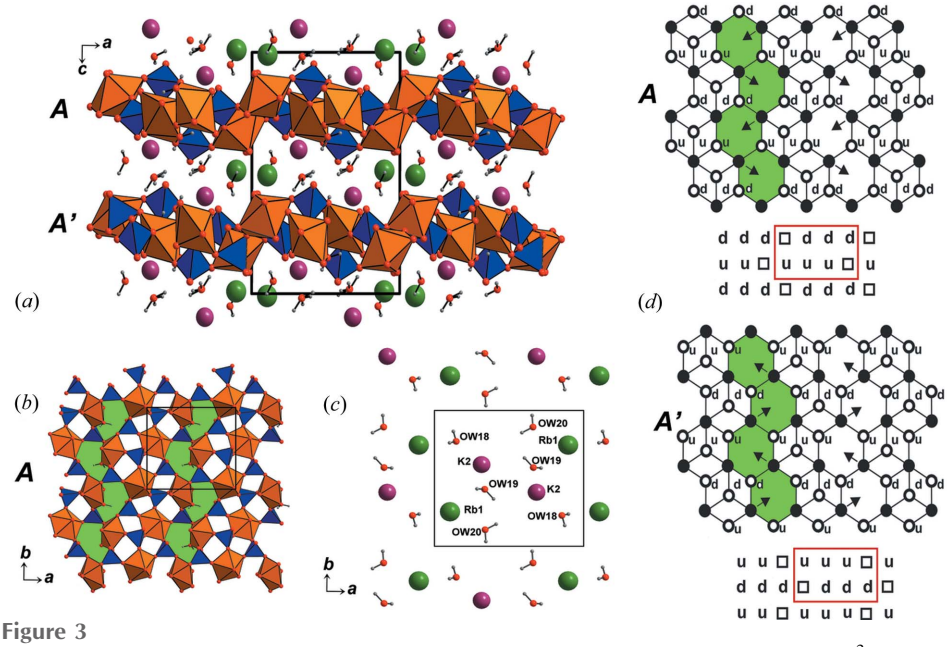

Figure 3
General projection of the structure of (2) (*a*). The unit cell contains two $[(UO_2)_2(CrO_4)_3H_2O]^{2-}$ layers *A* and *A*′. The layers are symmetrically identical and rotated by 180° relative to each other (*b*). Arrangement of alkaline atom sites and water molecules in the interlayer (*c*). Graphs of *A* and *A*′ layers with *u* and *d* symbols written near the white vertices (Cr atoms). Six-membered rings form edge-sharing chains (highlighted in green). Below the graphs the achiral orientation matrices are given.

3.2.3. $[(CH_3)_3CNH_3]_2[(UO_2)_2(CrO_4)_3H_2O]$ (3). The structure of

Table 5
Interpolyhedral U—O_{br}—Cr bond angles (°) in the structures of (1)–(3).

	(1)	(2)	(3)
Cr2—O_{br}1—U2	128.7 (4)	132.6 (4)	152.2 (4)
Cr1—O_{br}2—U2	140.6 (4)	137.5 (4)	130.6 (3)
Cr1—O_{br}6—U1	146.8 (4)	135.7 (4)	155.8 (3)
Cr1—O_{br}7—U1	163.9 (5)	141.5 (4)	146.0 (3)
Cr3—O_{br}8—U2	131.8 (5)	136.3 (4)	139.7 (3)
Cr2—O_{br}9—U1	135.4 (4)	134.1 (4)	137.8 (3)
Cr2—O_{br}10—U2	146.5 (5)	141.9 (4)	140.2 (4)
Cr3—O_{br}13—U1	153.4 (4)	133.5 (4)	141.0 (3)
Cr3—O_{br}15—U1	164.0 (5)	165.0 (5)	153.0 (3)

Table 6
Interpolyhedral U—O_{br}—Cr bond angles (°) in the structure of (4).

A-type layer		*B*-type layer	
Cr2—O_{br}1—U2	137.1 (8)	Cr6—O_{br}19—U4	153.7 (10)
Cr2—O_{br}9—U1	132.5 (7)	Cr6—O_{br}31—U3	141.5 (9)
Cr3—O_{br}13—U1	140.2 (6)	Cr5—O_{br}20—U3	149.1 (8)
Cr3—O_{br}8—U2	129.8 (7)	Cr5—O_{br}29—U4	139.4 (7)
U2—O_{br}1—Cr2	137.1 (8)	Cr4—O_{br}28—U4	137.7 (8)
Cr2—O_{br}10—U2	135.8 (9)	Cr4—O_{br}30—U4	155.6 (9)
Cr1—O_{br}6—U1	143.3 (6)	Cr4—O_{br}27—U3	144.7 (8)
Cr1—O_{br}7—U1	143.2 (8)	Cr6—O_{br}18—U3	138.0 (8)
Cr3—O_{br}15—U1	149.8 (8)	Cr5—O_{br}24—U3	134.4 (8)

(3) also contains two $[(UO_2)_2(CrO_4)_3(H_2O)]^{2-}$ layers *A* and *A*′ per unit cell (Fig. 4*a*). In contrast to (1), (2) and (4), it does not host water molecules in the interlayer. A probable intralayer hydrogen bonding system is characterized by distances O*W*17—O8 [3.06 (1) Å] and O*W*17—O9 [2.94 (1) Å] and an angle O8—O*W*17—O9 of about 103°. Since the aliphatic components of the *tert*-butylammonium cations are hydrophobic, their packing can be subdivided into hydrophobic and hydrophilic zones (Fig. 4*b*). Similar well defined hydrophobic and hydrophilic zones are absent in (1) and (4). Overall, the structure of (3) is very similar to the previously reported isopropylammonium uranyl chromate in Siidra *et al.* (2012*a*). In contrast to (1) and (2), the orientation matrices of *A* and *A*′ layers of (3) are different and chiral (Fig. 4*c*).

3.2.4. $[(CH_3)_2NH_2]_4[(UO_2)_2(CrO_4)_3H_2O]_2(H_2O)$ (4). Compared with (2) and (3), the *c* lattice parameter of (4) is nearly doubled (Table 2). Compound (4) crystallizes in the non-centrosymmetric space group $P2_12_12_1$ and contains four $[(UO_2)_2(CrO_4)_3(H_2O)]^{2-}$ layers per unit cell (Fig. 5*a*). There are no clearly recognizable hydrophobic and hydrophilic zones. The layers designated as *A* and *A*′ (Fig. 6) correspond to the general topology described above for (1), (2) and (3), with up-and-down orientations similar to that of (3) (Fig. 4*c*). *B* and *B*′ layers are formed by six-membered rings sharing corners to form chains separated by chains of four-membered rings. Indicators for probable intralayer hydrogen bonds are O*W*17—O8 2.79 (1), O*W*17—O9 2.90 (1) Å, angle O8—O*W*17—O9 107.6° for *A* layers, and O*W*34—O29 2.90 (2), O*W*34—O31 3.07 (2) Å, angle O29—O*W*34—O31 109.8° for *B* layers. The up-and-down orientations of chromate tetrahedra observed in the *B* layers of (4) have no analogues in the corresponding selenate or sulfate species which allow identifying this layer as a new geometrical isomer (Moore, 1970). Moreover, analysis of the orientations of H_2O vectors (marked by arrows on Fig. 6) near the 4-connected black vertices reveal its similarity to (1), (2) and (3). All CrO_4 tetrahedra along the directions of the H_2O vectors alternate in 'up' and 'down' orientation. The latter is different from *B* layers described in uranyl-selenates in Krivovichev *et al.* (2009), where all tetrahedra along these vectors point in the same orientation. Interpolyhedral U—O_{br}—Cr bond angles are very different for *A*-type and *B*-type layers in (4) (Table 6). Thus, the structure of (4) is formed by two topologically different types of $[(UO_2)_2(CrO_4)_3(H_2O)]^{2-}$ layers having an ...*ABA*′*B*′... stacking sequence. The formula can thus be written as $[(CH_3)_2NH_2]_4\{^A[(UO_2)_2(CrO_4)_3H_2O]^B[(UO_2)_2$-

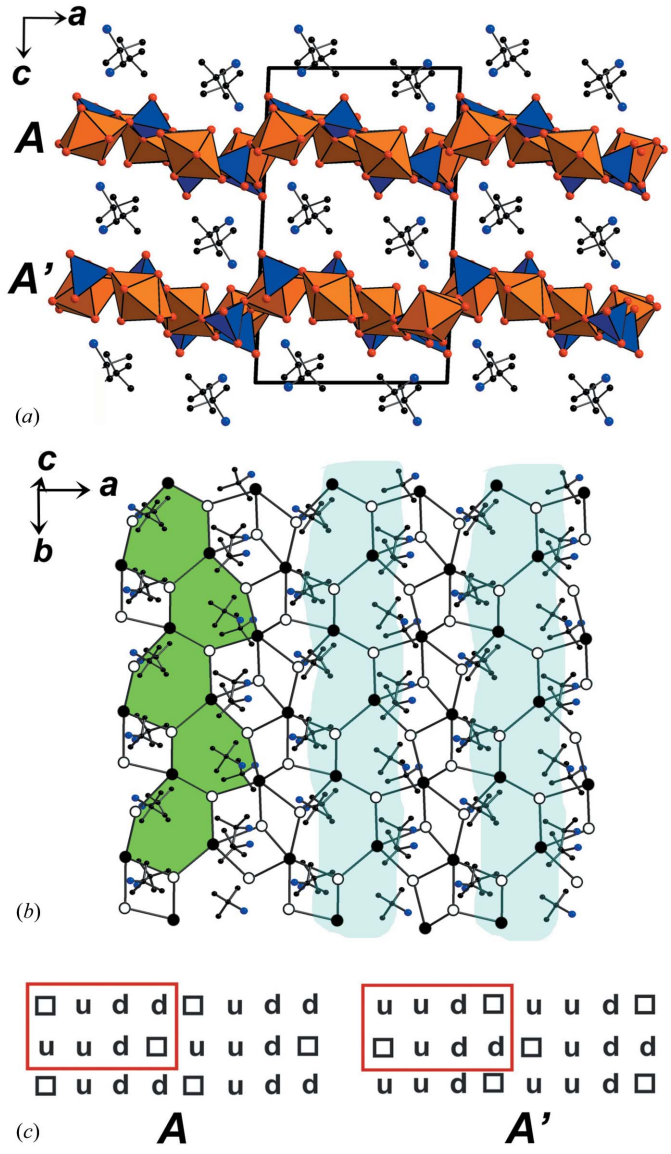

Figure 4
General projection of the structure of (3) (*a*). Similar to the structure of (2), there are two $[(UO_2)_2(CrO_4)_3H_2O]^{2-}$ *A* and *A*′ layers per unit cell. Graph of the inorganic layer with the skeletons of the *tert*-butylammonium cations of the interlayer space projected onto the graph. In the interlayer space hydrophobic (highlighted by light-blue) and hydrophilic zones can be distinguished. (*b*) Chiral orientation matrices of *A* and *A*′ layers (*c*).

$(CrO_4)_3H_2O]\}(H_2O)$. The negative charge of the $^{A}[(UO_2)_2(CrO_4)_3H_2O]^{2-}$ layer is compensated by two symmetrically independent DMA molecules, whereas that of $^{B}[(UO_2)_2(CrO_4)_3H_2O]^{2-}$ is compensated by another two different DMA molecules.

4. Discussion

The structural topologies of layers in (1), (2), (3) and (4) are similar to those previously reported for uranyl selenates, uranyl sulfates and uranyl chromates (Thomas *et al.*, 2003; Doran *et al.*, 2003, 2004; Krivovichev *et al.*, 2009; Siidra *et al.*, 2012*a*). The structure of (2) is the first example of $[(UO_2)_2(T^{6+}O_4)_3(H_2O)]^{2-}$ (T = S^{6+}, Cr^{6+}, Se^{6+}) layer formation in uranyl-based compounds with inorganic cations only. Moreover, it is also the first uranyl chromate simultaneously containing two different alkali metals. Note that $K_2[(NpO_2)_2(CrO_4)_3(H_2O)](H_2O)_3$ was described previously in a neptunyl-containing system (Grigor'ev *et al.*, 2004). *B* layers as observed in (4) have not been described before in uranyl chromates, but were also found in several neptunyl chromates

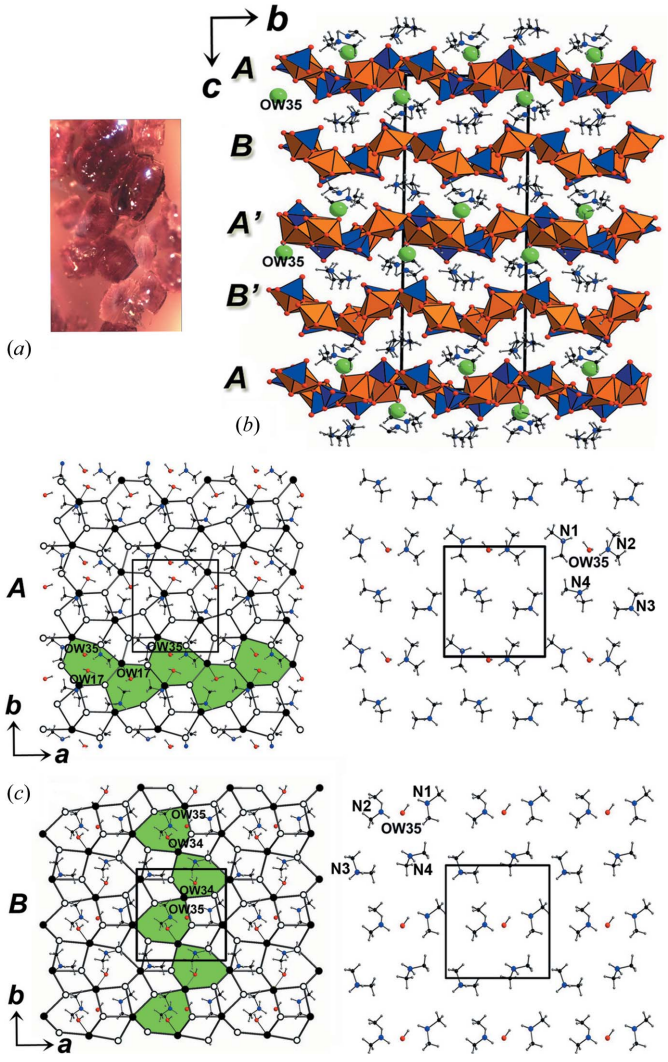

Figure 5
Crystals of (4) as obtained by a combination of hydrothermal and evaporation methods (*a*). General projection of the crystal structure of (4) along the *c* axis. *OW*35 water molecule sites are highlighted by large green balls. Four *A*, *A*′, *B* and *B*′ $[(UO_2)_2(CrO_4)_3H_2O]^{2-}$ layers are present per unit cell (*b*). Graphs of the inorganic layer with projection of the interlayer space beneath (*c*). Interlayer *OW*35 water molecules are located under every second six-membered ring (highlighted in green). Chains formed by edge-sharing (in *A* and *A*′ layers) and corner-sharing (in *B* and *B*′ chains) six-membered rings are mutually perpendicular.

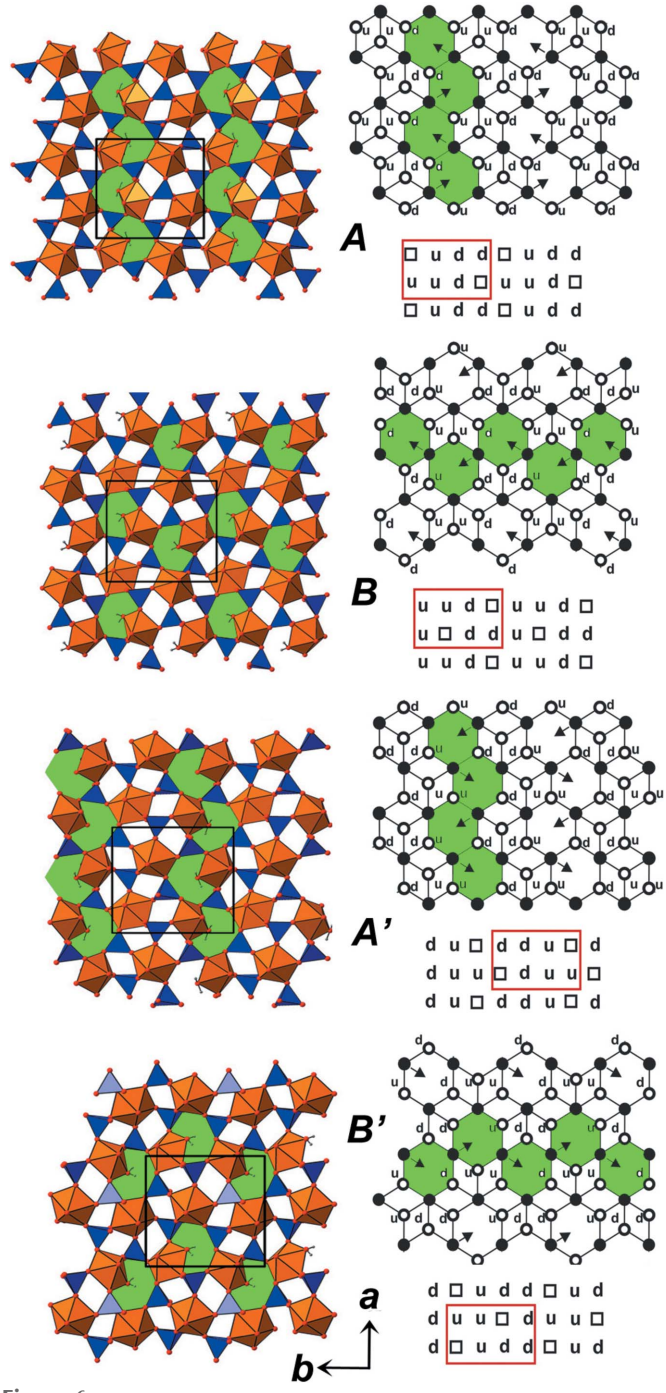

Figure 6
General projection of *A*, *A*′, *B* and *B*′ layers in the structure of (4). Graphs with *u* and *d* symbols written near the white vertices (Cr atoms). Six-membered rings form edge-sharing (*A* and *A*′ layers) and corner-sharing (*B* and *B*′ layers) chains (highlighted in green). Below the graphs chiral orientation matrices are given.

(Budantseva *et al.*, 2003). The structural architecture of (4) formed by layers of different topology is unique. In Krivovichev *et al.* (2009) during the study of uranyl selenates it was suggested that layers with *B* topology were formed when organic cations with long-chained alkyl-ammonium groups are present, but *A* layers preferred formation with shorter ones. However, the current study demonstrates that even with short-chained alkyl-ammonium groups both types of topologies may be formed. It is a new finding that the type *A* layer topology can also exist in a non-centrosymmetric space group. From these different experimental facts it is not easy to build a convincing concept able to predict or to explain the preference for one of the two layer topologies *A* and *B*.

Both compounds (1) and (4) contain DMA cations, but the resulting structural architectures are different. The structure of (4) can be imagined as the intercalation of neutral $\{[(CH_3)_2NH_2]_2^{B}[(UO_2)_2(CrO_4)_3H_2O]\}$ and $\{[(CH_3)_2NH_2]_2^{B'}[(UO_2)_2(CrO_4)_3H_2O]\}$ blocks into the stacking of likewise neutral $\{[(CH_3)_2NH_2]_2^{A}[(UO_2)_2(CrO_4)_3H_2O](H_2O)\}$ and $\{[(CH_3)_2NH_2]_2^{A'}[(UO_2)_2(CrO_4)_3H_2O](H_2O)\}$ blocks. The resulting organic interlayer contains four symmetrically independent DMA cations (Fig. 5*c*). The possibility to form a similarly stable phase with an anhydrous interlayer is demonstrated by the example of (3).

It is of interest to consider the formation of possible hydrogen bonding between water molecules in the interlayer and $[(UO_2)_2(CrO_4)_3(H_2O)]^{2-}$ layers in the structures of (1), (2) and (4) as these reveal considerable differences. O—H···O distances for interlayer water molecules are listed in Table 7 and are indicative of hydrogen bonding of different strength (strong 2.2–2.5 Å; moderate 2.5–3.2 Å; weak > 3.2 Å; Steiner, 2002). Moderate hydrogen bonds of O*W*18 molecules are formed to O12 atoms being terminal in CrO_4 tetrahedra and weakly bonded to O2 atoms which are bridging between CrO_4 and UrO_5 in the structure of (1). (Fig. 7*a*). In contrast to (1) three different water molecules in the centrosymmetric structure of (2) are bonded (Fig. 7*b*) to both upper and lower

Table 7
$d(D\cdots A)$ distances for interlayer water molecules in the structures of (1), (2) and (4).

D—H	$d(D\cdots A)$	D—H	$d(D\cdots A)$
(1)		(2)	
*OW*18—*HW1C*···O_t12	2.95 (1)	*OW*18—*HW1C*···O_{br}6	2.91 (1)
*OW*18—*HW1D*···O_{br}2	3.23 (1)	*OW*18—*HW1D*···O_{br}3	2.85 (1)
		*OW*18—*HW1D*···O_{br}5	3.19 (1)
(4)		*OW*19—*HW1E*···O_{br}2	2.86 (1)
*OW*35—*HW3E*···O_{br}5	3.16 (1)	*OW*19—*HW1F*···O_t12	3.31 (1)
*OW*35—*HW3E*···O_{br}13	2.93 (1)	*OW*19—*HW1F*···*OW*20	3.15 (1)
		*OW*20—*HW1A*···O_{br}1	3.39 (1)
		*OW*20—*HW1A*···O_{br}9	2.82 (1)
		*OW*20—*HW1B*···O_{br}1	2.86 (1)
		*OW*20—*HW1B*···O_t12	3.34 (1)

A and *A*′ layers. There is only one symmetrically independent H_2O molecule in the structure of (4). During the analysis of the structural architecture of (4) it was found that O*W*35 water molecules in the interlayer are bonded exclusively to *A* and *A*′ layers (Figs. 5*a* and 7*c*). O*W*35 molecules are located under every second six-membered ring (Fig. 5*b*) and bonded to O atoms of *A* and *A*′ layers (Fig. 7*c*) than to *B* and *B*′. Thus, the location of O*W*35 molecules, preferential hydrogen bonding with *A*-type layers and steric hindrance make the structure of (4) non-centrosymmetric. The character of hydrogen bonding in (4) is somewhat similar to the structure of (1).

From the analysis of interatomic distances and angles it is highly probable that in all considered layers, *A* or *B*, intralayer hydrogen bonds of moderate strength between the sole water molecule of the $UrO_4(H_2O)$ polyhedra and bridging O atoms are also formed. However, from the mere fact that the same *A* layer topology was found for all four studied compounds it is highly probable that the formation of the $[(UO_2)_2(CrO_4)_3(H_2O)]^{2-}$ layers occurs on the basis of their own high degree of stability, but the nature of the interlayers seems to play an important role in 'fine-tuning' the details, *e.g.* determination of the orientation pattern of the CrO_4 tetrahedra including the chirality or achirality of the layers, the space-group symmetry and the corrugation of the layers.

Both (3) and (4) contain chiral layers and, interestingly, these layers are formed from achiral building units. This is somewhat analogous to certain organic compounds, where also achiral molecules are able to form chiral layers (Tanaka *et al.*, 2006; Gong *et al.*, 1999). Within the concept of such an interpretation the structure of (3) can then be described as a racemate consisting of two *A* and *A*′ chiral layers which are mirror images of each other reflected in the *ac* plane. In a similar approach the structure of (4) can be interpreted as being formed by four chiral layers. Layer pairs *AA*′ and

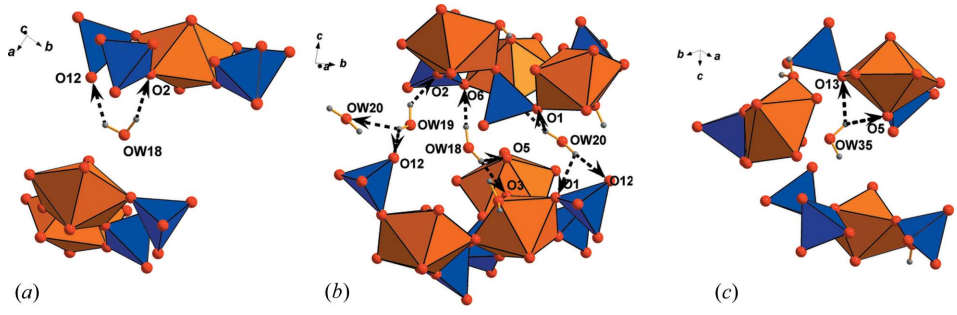

Figure 7
Possible hydrogen bonding of interlayer H_2O molecules in the structures of (1) (*a*), (2) (*b*) and (4) (*c*). H_2O (O*W*18 site) molecules are moderately bonded with O12 atoms being terminal in CrO_4 tetrahedra and weakly bonded to O2 atoms bridging between CrO_4 and UrO_5 in the structure of (1). Hydrogen bonds of H_2O (O*W*18, O*W*19, O*W*20) molecules with O atoms of both *A* and *A*′ $[(UO_2)_2(CrO_4)_3H_2O]^{2-}$ layers are formed in the structure of (2). Hydrogen bonds from O*W*35 water molecules are formed exclusively to O atoms of *A* and *A*′ layers, whereas hydrogen bonds to *B* and *B*′ layers are absent in the structure of (4). Amine molecules and K, Rb sites in the interlayers are omitted for clarity. See text for details.

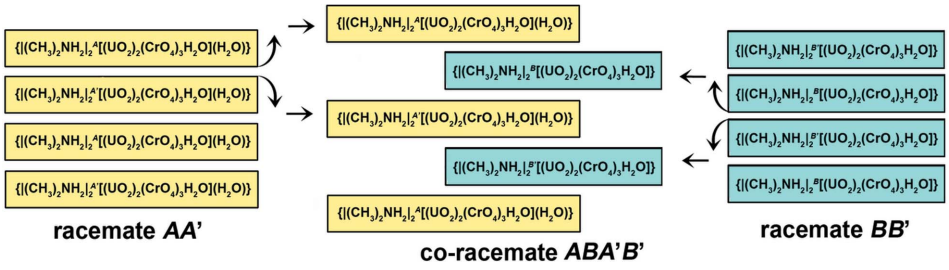

Figure 8
The structure of (4) can be imagined as a co-racemate formed by intergrowth of racemic AA' blocks (yellow) and racemic BB' blocks (blue).

BB' can then be considered as racemic pairs and the whole structure would be called a co-racemate built by a combination of two racemates (Fig. 8). Even in organic chemistry the occurrence of co-racemates seems to be a rare event as we have found only one report in the literature (Qin *et al.*, 2016).

5. Conclusion

A and *B* topologies of $[(UO_2)_2(T^{6+}O_4)_3(H_2O)]^{2-}$ (T = S^{6+}, Cr^{6+}, Se^{6+}) layers discussed above are one of the most stable and abundant structural architectures in uranyl-based systems with various organic and alkali cations. The structures of (2) and (3) are similar to those previously reported in the uranyl-selenate and uranyl-sulfate systems, probably because S^{6+}, Cr^{6+} and Se^{6+} cations have very similar ionic radii and their tetrahedral oxoanions play a similar topological role in structure self-assembly processes. The unique structural configurations and non-centrosymmetry in (1) and (4) is arguably governed by the selective formation of hydrogen bonding rather than by the formation of hydrophobic and hydrophilic zones in the organic interlayer. Chiral architectures in uranyl systems may form from achiral building units, as observed in (3) and (4).

In the overwhelming number of previously reported cases racemates are formed during the spontaneous resolution of enantiomers and the absence of chirality sources (Pérez-García & Amabilino, 2002). Thus, tentatively a two-stage formation can be suggested for (4). Clusters of the first racemate were formed during the first hydrothermal stage, but did not reach the critical size of stable nuclei, but served as a chiral template for the formation of the second racemate during the low-temperature stage. It is difficult to suggest which racemate was the first to form, since the complexity of both of them is very similar. Thus, a two-stage formation process as well as steric hindrance effects may explain the unique layered packing of (4) ($\ldots ABA'B' \ldots$).

Acknowledgements

This work was financially supported by the Russian Science Foundation through the grant 16-17-10085. Technical support by the SPbSU X-ray Diffraction Resource Centre is gratefully acknowledged.

References

Bacsik, Z., Mink, J. & Zou, X. (2008). *Nat. Mater.* **7**, 381–385.
Bharara, M. S. & Gorden, A. E. V. (2010). *Dalton Trans.* **39**, 3557–3559.
Budantseva, N. A., Andreev, G. B., Fedoseev, A. M. & Antipin, M. Yu. (2003). *Russ. J. Coord. Chem.* **29**, 653–657.
Burns, P. C. & Finch, R. J. (1999). *Am. Mineral.* **84**, 1456–1460.
Carrión, M. C., Ortiz, I. M., Jalón, F. A., Manzano, B. R., Rodríguez, A. M. & Elguero, J. (2011). *Cryst. Growth Des.* **11**, 1766–1776.
Davis, M. E. (2014). *Chem. Mater.* **26**, 239–245.
Dembowski, M., Olds, T. A., Pellegrini, K. L., Hoffmann, C., Wang, X., Hickam, S., He, J., Oliver, A. G. & Burns, P. C. (2016). *J. Am. Chem. Soc.* **138**, 8547–8553.
Dong, D., Yu, N., Zhao, H., Liu, D., Liu, J., Li, Z. & Liu, D. (2016). *J. Mol. Struct.* **1104**, 58–62.
Doran, M., Norquist, A. J. & O'Hare, D. (2002). *Chem. Commun.* pp. 2946–2947.
Doran, M. B., Norquist, A. J. & O'Hare, D. (2003). *Inorg. Chem.* **42**, 6989–6995.
Doran, M. B., Norquist, A. J., Stuart, C. L. & O'Hare, D. (2004). *Acta Cryst.* E**60**, m996–m998.
Dryzun, C., Mastai, Y., Shvalb, A. & Avnir, D. J. (2009). *J. Mater. Chem.* **19**, 2062–2069.
Dubbeldam, D., Calero, S. & Vlugt, T. J. H. (2014). *Mol. Simul.* **40**, 585–598.
Finch, R. J., Burns, P. C., Hawthorne, F. C. & Ewing, R. C. (2006). *Can. Mineral.* **44**, 1197–1205.
Flack, H. D. (1983). *Acta Cryst.* A**39**, 876–881.
Gao, E.-Q., Yue, Y.-F., Bai, S.-Q., He, Z. & Yan, C.-H. (2004). *J. Am. Chem. Soc.* **126**, 1419–1429.
Gong, B., Zheng, C., Zeng, H. & Zhu, C. (1999). *J. Am. Chem. Soc.* **121**, 9766–9767.
Grigor'ev, M. S., Fedoseev, A. M., Budantseva, N. A., Bessonov, A. & Krupa, J.-C. (2004). *Crystallogr. Rep.* **49**, 598–602.
Gu, Z.-G., Zhan, C., Zhang, J. & Bu, X. (2016). *Chem. Soc. Rev.* **45**, 3122–3144.
Krivovichev, S. V., Burns, P. C. & Tananaev, I. G. (2007). Editors. *Structural Chemistry of Inorganic Actinide Compounds*. Amsterdam: Elsevier.
Krivovichev, S. V., Cahill, C. L., Nazarchuk, E. V., Burns, P. C., Armbruster, Th. & Depmeier, W. (2005). *Microporous Mesoporous Mater.* **78**, 209–215.
Krivovichev, S. V., Gurzhiy, V. V., Tananaev, I. G. & Myasoedov, B. F. (2009). *Z. Kristallogr.* **224**, 316–324.
Lacasta, S., Sebastián, V., Casado, C., Mayoral, A., Romero, P., Larrea, A., Vispe, E., López-Ram-de-Viu, P., Uriel, S. & Coronas, J. (2011). *Chem. Mater.* **23**, 1280–1287.
Leus, K., Liu, Y.-Y. & Van Der Voort, P. (2014). *Catal. Rev.* **56**, 1–56.
Li, J.-R., Sculley, J. & Zhou, H.-C. (2012). *Chem. Rev.* **112**, 869–932.
Li, Y., Xu, G., Zou, W.-Q., Wang, M.-S., Zheng, F.-K., Wu, M.-F., Zeng, H.-Y., Guo, G.-C. & Huang, J.-S. (2008). *Inorg. Chem.* **47**, 7945–7947.
Ling, J., Sigmon, G. E. & Burns, P. C. (2009). *J. Solid State Chem.* **182**, 402–408.
Liu, J., Chen, L., Cui, H., Zhang, J., Zhang, L. & Su, C.-Y. (2014). *Chem. Soc. Rev.* **43**, 6011–6061.
Mallick, A., Saha, S., Pachfule, P., Roy, S. & Banerjee, R. (2010). *J. Mater. Chem.* **20**, 9073–9080.

Marsh, R. E. (1995). *Acta Cryst.* B**51**, 897–907.
Moore, P. B. (1970). *Neues Jahrb. Miner. Monat.* **1970**, 163–173.
Nazarchuk, E. V., Siidra, O. I., Krivovichev, S. V., Malcherek, T. & Depmeier, W. (2009). *Z. Anorg. Allg. Chem.* **635**, 1231–1235.
Nazarchuk, E. V., Siidra, O. I., Zadoya, A. I. & Agakhanov, A. A. (2015). *Inorg. Chem. Commun.* **62**, 15–18.
Ou, S. & Wu, C.-D. (2014). *Inorg. Chem. Front.* **1**, 721–734.
Pérez-García, L. & Amabilino, D. B. (2002). *Chem. Soc. Rev.* **31**, 342–356.
Plášil, J., Fejfarová, K., Dušek, M., Škoda, R. & Rohlíček, J. (2013). *Am. Mineral.* **98**, 549–553.
Qin, L.-F., Pang, C.-Y., Han, W.-K., Zhang, F.-L., Tian, L., Gu, Z.-G., Ren, X. & Li, Z. (2016). *Dalton Trans.* **45**, 7340–7348.
Sheldrick, G. M. (2015). *Acta Cryst.* C**71**, 3–8.
Siidra, O. I., Nazarchuk, E. V., Kayukov, R. A., Bubnova, R. S. & Krivovichev, S. V. (2013). *Z. Anorg. Allg. Chem.* **639**, 2302–2306.
Siidra, O. I., Nazarchuk, E. V. & Krivovichev, S. V. (2012*a*). *Z. Anorg. Allg. Chem.* **638**, 976–981.
Siidra, O. I., Nazarchuk, E. V. & Krivovichev, S. V. (2012*b*). *Z. Kristallogr.* **227**, 530–534.
Siidra, O. I., Nazarchuk, E. V. & Krivovichev, S. V. (2012*c*). *Z. Anorg. Allg. Chem.* **638**, 982–986.
Siidra, O. I., Nazarchuk, E. V., Petrunin, A. A., Kayukov, R. A. & Krivovichev, S. V. (2012). *Inorg. Chem.* **51**, 9162–9164.
Siidra, O. I., Nazarchuk, E. V., Suknotova, A. N., Kayukov, R. A. & Krivovichev, S. V. (2013). *Inorg. Chem.* **52**, 4729–4735.
Siidra, O. I., Nazarchuk, E. V., Sysoeva, E. V., Kayukov, R. A. & Depmeier, W. (2014). *Eur. J. Inorg. Chem.* **2014**, 5495–5498.
Steiner, T. (2002). *Angew. Chem. Int. Ed.* **41**, 48–76.
Tanaka, A., Inoue, K., Hisaki, I., Tohnai, N., Miyata, M. & Matsumoto, A. (2006). *Angew. Chem.* **118**, 4248–4251.
Tang, L., Shi, L., Bonneau, C., Sun, J., Yue, H., Ojuva, A., Lee, B.-L., Kritikos, M., Bell, R. G. & Comyns, A. E. (2011). *Microporous Mesoporous Mater.* **138**, 243.
Thomas, P. M., Norquist, A. J., Doran, M. B. & O'Hare, D. (2003). *J. Mater. Chem.* **13**, 88–92.
Wang, S., Alekseev, E. V., Ling, J., Liu, G., Depmeier, W. & Albrecht-Schmitt, T. E. (2010). *Chem. Mater.* **22**, 2155–2163.
Xu, Z.-X., Ma, Y.-L. & Zhang, J. (2016). *Chem. Commun.* **52**, 1923–1925.
Yu, J. & Xu, R. (2008). *J. Mater. Chem.* **18**, 4021–4030.
Zhang, L. & Jiang, J. (2011). *J. Membr. Sci.* **367**, 63–70.